Experimental investigation of soot production in a confined swirled flame operating under perfectly premixed rich conditions

Mathieu Roussillo, Philippe Scouflaire, Sebastien Candel, Benedetta Franzelli

Experimental investigation of soot production in a confined swirled flame operating under perfectly premixed rich conditions

Mathieu ROUSSILLO[a,b,*], Philippe SCOUFLAIRE[a], Sébastien CANDEL[a], Benedetta FRANZELLI[a]

[a] *Laboratoire EM2C, CNRS, CentraleSupélec, Université Paris-Saclay 3 Rue Joliot Curie 91192 Gif-sur-Yvette Cedex France*
[b] *Centre de Recherche Paris-Saclay — Air Liquide, 1 Chemin de la Porte des Loges, 78350 Les Loges-en-Josas, France*

Abstract

A detailed understanding of the mechanisms underlying soot production is needed to control particle emissions from practical combustion devices. This requires fundamental investigations of these processes in turbulent combustion systems. This study reports experiments on soot production in a perfectly premixed turbulent flame operating under rich conditions. A swirled ethylene/air flame is stabilized in a confined combustor at atmospheric pressure with full optical access. Quantitative measurements of the soot volume fraction (f_v) are carried out with the Laser Induced Incandescence (LII) technique, allowing the characterization of the soot spatial distribution and temporal intermittency. While f_v is detected by LII mainly in the near-wall region of the burner, light scattering measurements bring complementary information on the presence of particles in the whole chamber. The investigation of a rich perfectly premixed turbulent flame represents an unexplored configuration that provides new insights on soot production in a situation where this process is not dominated by mixing between fuel and air. The data gathered in this situation may be of interest in future developments of modeling methods and their validation for soot prediction.

Keywords:
Soot, Laser Induced Incandescence, Light Scattering, Rich premixed swirled flame

*Corresponding author:
Email address: mathieu.roussillo@centralesupelec.fr
(Mathieu ROUSSILLO)

1. Introduction

Soot emission is now recognized as an important issue for its adverse effects on climate [1] and human health [2]. The problem is not easy to solve because soot is produced by complex processes and the difficulties are compounded by the fact that most practical devices involve turbulent flames. Numerical simulations are still not capable of precisely predicting soot production [3] and it is important to advance soot modeling to help the control and reduction of soot emission from these systems. In addition to the many studies carried out on sooting laminar flames, it is worth examining soot production in turbulent flows that are widely used in industrial applications. In this respect, much of the technical literature has focused on soot in turbulent jet diffusion flames [4–8]. This case has been extensively investigated with a variety of diagnostics, highlighting the effects of turbulent eddies, strain rate and scalar dissipation on the soot volume fraction f_v distribution. Recently, Geigle et al. [9, 10] have developed a confined swirled turbulent non-premixed configuration, providing new insights on soot production in a system that has many of the features found in industrial burners. However, all these investigations deal with the non-premixed combustion mode, where soot production is essentially controlled by the quality of mixing between fuel and oxidizer that is mainly governed by the turbulence. The local mixture inhomogeneities dominate the soot production process, complicating the interpretation of the experimental data and numerical modeling of soot production.

It was then worth asking whether one could study soot production in a turbulent flame operating under perfectly-premixed rich conditions. This has led to the development of the "EM2Soot" burner, in which a rich premixed swirled turbulent flame is established in an optically accessible combustor [11]. The interest of this experimental burner is threefold. First, it allows to independently examine effects of various parameters on soot production such as the equivalence ratio or the flame power, bypassing the complexities linked to the presence of local mixture inhomogeneity [11]. Second, this configuration can be used to generate a new experimental database for the validation of soot modeling in turbulent flames. In particular, the perfectly premixed rich flame represents an unexplored situation which complements the experimental database of the International Sooting Flame (ISF) workshop [12]. To this end, ethylene, the reference fuel for the ISF activities, is here retained due to its high propensity to produce soot and the large availability of models for sooting ethylene flame simulations. Third, the investigated rich premixed flames provide information that may be of interest in the design of combustors employing Rich-Quench-Lean (RQL) concepts to reduce pollutant emissions, in which the first stage combustion process is carried out in a rich regime at an equivalence ratio $\phi \simeq 1.8$.

In the present work, soot production in the EM2Soot configuration is characterized and this is, to our knowledge, a first of this kind. The experimental setup is briefly introduced in Section 2, together with the Laser Induced Incandescence (LII) and Laser Light Scattering (LS) techniques employed to investigate soot volume fraction and soot particle presence, respectively. Soot production is then characterized in Section 3, by examining the volume fraction distribution, and the spatially layered structure of soot particles. Using light scattering imaging it is also shown that soot particles are present in some regions where their volume fraction is below the detection threshold of LII. Section 3 then discusses the temporal variability of soot volume fraction induced by the turbulent eddies.

2. Experimental Setup

A detailed description of the EM2Soot burner may be found in [11] and is only summarized in what follows. The burner, schematically represented in Fig. 1a, includes three components: the plenum, the injector and the combustion chamber. The chamber features a square cross section and its dimensions are 118 × 118 × 250 mm^3. An ethylene/air mixture at ambient temperature prepared in the upstream manifold is conveyed to a plenum feeding an injection channel equipped with a radial swirler (Swirl number $S = 0.7$). It is formed by four quartz windows (90 mm × 250 mm × 3 mm) mounted between metallic corner pieces. One of the corner bars is equipped with 8 thermocouples measuring the temperature on the inner side of the chamber wall. The burner can be operated in a large domain of equivalence ratios and mass flow rates, but this study focuses on the reference operating conditions summarized

ϕ	P_{tot} (kW)	$\dot{m}_F$ (g/s)	$\dot{m}_{air}$ (g/s)	Re
2.1	15	0.319	2.23	20000

Table 1: Reference flame operating conditions: equivalence ratio, flame power, fuel and air mass flow rates, Reynolds number.

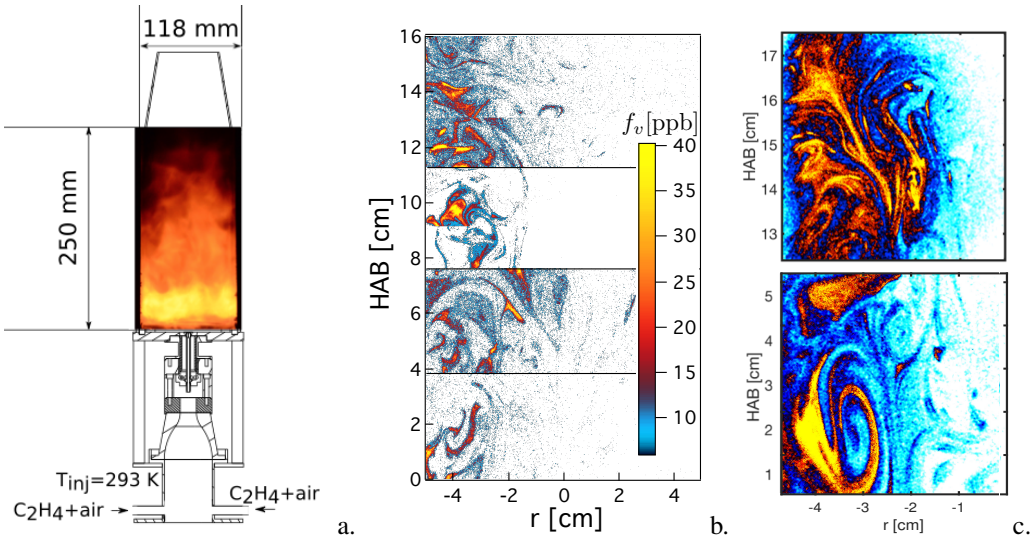

Figure 1: (a) Schematic of the EM2Soot burner. (b) 2-D mapping of instantaneous soot volume fraction by LII as a selective collage of images recorded at different heights (pixel size Δx = 0.1 mm). (c) Close-up views of soot structure at two HABs: the camera is equipped with an extension ring (Δx = 0.05 mm).

in Table 1, chosen for the high soot production of the corresponding flame. In this configuration, soot generation is strongly dependent on the wall temperature [11]. It is therefore ensured that all experiments are carried out at a fixed initial wall temperature (T = 573 K measured by one of the thermocouples at a height above the burner HAB=113 mm), which is obtained by preheating the chamber with a lean flame to prevent quartz obscuration by soot deposits. During each experimental run, corresponding to a duration of about 30 s, the wall temperature varies by less than 3% so that a quasi-steady state can be assumed for the thermal environment. In addition, using a short acquisition time the soot deposit on the wall can be considered to be negligible during each experimental run.

The broadband emission of light from the reference flame, recorded by a Nikkon D700 camera, is displayed in Fig. 1a. Light is emitted from a large volume of the chamber, but the largest intensities originate from the lower part, where a highly luminous yellow flame is observed. One may then deduce that soot concentration is mainly present in the vicinity of the chamber bottom plane. However, the detected signal also depends on the soot temperature through Planck's law so that the intensity only provides a qualitative indication of the presence of soot.

It is then more instructive to deduce 2-D soot volume fraction fields from LII techique since the LII signal is effectively proportional to soot volume fraction [13]. The detection performance of this technique depends on the laser characteristics and on the optical setup, allowing to capture the presence of soot only when f_v exceeds a critical threshold value ϵ (here ϵ = 7.5ppb). Light scattering (LS) imaging is also used in the present investigation as a complementary optical diagnostic. Its physical interpretation is less easy since the scattered light signal is not directly proportional to f_v, being strongly dependent on particle morphology and sizes [14]. For this reason, the LS images are essentially used as an indication of soot presence and of the spatial layout of soot. As the sensitivity of LS is not linked to the volume fraction value, it can be used to detect the presence of soot particles in regions where $f_v < \epsilon$.

LII measurements are performed using a laser sheet focused on the burner central axis (convergent lens f=+1000, cylindric lens f=-50), obtained from a Nd:YAG laser (1064 nm, 10 Hz). The sheet is 0.35 mm thick and extends over 7 cm in the vertical direction. It should be noticed that a uniform fluence is guaranteed only in the central 4 cm of this laser sheet. The laser fluence is set to approximately 0.45 J/cm^2 with a shot duration of $\approx$ 9 ns. This value belongs to the "plateau" region [15] of the LII signal for this configuration [11].

LS measurements are performed using a 9 cm wide laser sheet generated with a Nd:YAG laser doubled to 532 nm with a shot duration of $\approx$ 9 ns. A low energy fluence (0.09 J/cm^2) is imposed to avoid soot incandescence.

The LII and LS signals are captured with two intensified CCD cameras (Princeton, PI-MAX 3, f=10Hz) and stored into a 3-D matrix: $I(x, y, t) \in \mathbf{R}_+^{N_x \times N_y \times N_t}$, with

$N_x = 1024$, $N_y = 1024$ and $N_t = 300$, defining a pixel size of 0.1mm. Close-up views are also obtained with a pixel size of 0.05mm by inserting an extension ring to the camera objective. Both cameras are equipped with Nikkor 50 mm f/2 lenses. A bandpass filter centered at 425 nm (50 nm FWHM) is used for LII to reduce parasitic C_2 Swan band emission and flame luminosity [16], whereas a bandpass filter centered at 532 nm is used for LS. A reliable proportionality between LII signals and soot volume fraction is achieved by suitably choosing the acquisition duration of the LII signal [13]. The signal is recorded with no delay with respect to the end of the laser pulse over a period of 100 ns to maximize the signal to noise ratio. The LS signal is acquired for 20 ns without delay with respect to the laser pulse. The LII signal has been calibrated via the Modulated Absorption Emission technique (MAE [17]) on a laminar diffusion flame [18], fixing the value of the soot complex refractive index $E(m, 645\ nm) = 0.38$. It is known that uncertainties in the value of $E(m)$ may lead to a relative error on the soot volume fraction that may be up to a factor two [18].

3. Characterization of soot production

3.1. Soot structure

Images of the LII signal in the form of instantaneous soot volume fraction fields along the chamber are displayed in Fig. 1b. It is worth noting that the laser beam enters the chamber from the left side. A net reduction in the intensity level can be observed on the right side, providing an indication on the soot absorption of the laser sheet as it travels in the chamber. Measurements in the right side of the flame are biased and the left side results are only considered in the following. Examining the LII signal, one notices that large volume fractions of soot are mainly present near the wall[1] Images indicate that the f_v values are generally below the LII detection threshold in the flame central region. Instantaneous f_v values can reach about 0.1 ppm near the wall ($|r| > 3$ cm) close to the bottom plane (HAB< 4 cm), which is fairly small compared to the levels classically observed in turbulent non-premixed flames [4, 7]. Further downstream, the level of instantaneous f_v generally decreases. Soot volume fraction appears in the form of layers of approximately 0.5-2.5 mm thickness, which are clearly distinguishable and comparable to previous

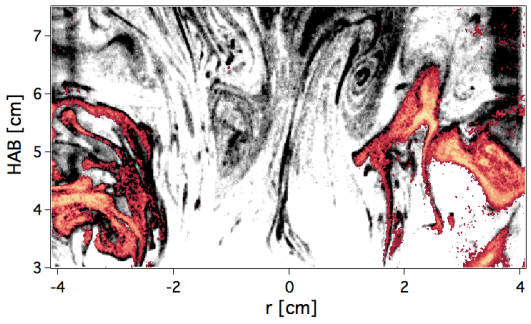

Figure 2: Simultaneous measurements of soot presence by LII (red) and LS (black) at $\lambda = 532$ nm.

experiments [4, 6]. A close-up view of these ligaments is presented for two HABs in Fig. 1c. The effect of turbulent eddies on the ligaments is quite visible, as they are wrinkled and distorted by the turbulent flow. Close to the injection plane (bottom image in Fig. 1c), larger eddy structures can be observed, so that soot particles occupy a reduced surface area, i.e. a high preferential concentration of soot particles prevails. Downstream (top image in Fig. 1c), large eddy structures are less visible reducing the preferential concentration of soot.

One may note that the spatial soot organization differs from that observed in the swirled non-premixed flame investigated by Geigle et al. [10, 19], which to our knowledge represents the only experimental database available in the literature for confined swirled sooting flames. This is most likely due to the different combustion modes. In particular, soot appears near the chamber walls in the present configuration in contrast with the pattern obtained in the DLR flame where f_v reaches its largest levels in the middle of the chamber and is nearly negligible in the outer recirculation zone close to the walls. Soot ligaments are also shorter than those found in the present experiment but both configurations feature a high spatial preferential concentration of soot, also designated as spatial intermittency. In the DLR flame, soot presence is related to the mixture fraction field and is linked to locally rich zones promoting soot production. The spatial distribution of soot then depends on turbulent mixing. In the present premixed flame, soot production is not governed by the local equivalence ratio since it is homogeneous in the whole chamber. Here, soot is expected to be mainly affected by the turbulence through fresh and burnt gas mixing, its effects on local flame properties (such as temperature or soot precursor concentration) and the stretch induced on soot ligaments by turbulent eddies.

Spatial soot structures are now investigated by exam-

[1] The immediate vicinity of the wall is not accessible due to the limitation of the optical access, reducing the field of view by about 5 mm for each side.

ining LS images [6] to collect information on soot presence and complement the LII data. This is exemplified with quasi-simultaneous measurements of LS and LII performed with the same laser sheet generator with two Nd:YAG lasers doubled to 532 nm. Light scattering is measured with a first low energy laser shot 20 ns before the LII shot to prevent any parasitic LII signal and vaporization of smallest soot particles. Results are displayed in Fig. 2. The LII signal (red) only features a few ligaments close to the wall as it pertains to sufficiently high detectable values of f_v. The LS signal (black) is superimposed on the LII signal where this signal is present but also recovers more soot ligaments everywhere in the chamber. These ligaments may be constituted by a small number of large aggregates or a big number of nuclei particles, so that the total soot volume fraction is negligible and therefore not detectable by the LII. At this point, it is not possible to know which is the correct interpretation. However, since light scattering of spherical particles in the Rayleigh regime is proportional to d_p^6, the first proposition, i.e. small number of large aggregates with bigger primary particle diameter d_p compared to soot nuclei, seems more likely but there is no clear proof of it at this stage. This point might be resolved in the future by performing time-gated LII measurements [18]. A 2-D instantaneous field of light scattering is displayed in Fig. 3a. by combining two uncorrelated images. Long soot ligaments highly wrinkled by the turbulent eddies are detected in the whole region. By comparing LII and LS instantaneous results (Figs. 1b and 3a, respectively), it can be deduced that sufficiently high values of f_v prevail along the walls, but soot particles are actually present everywhere in the chamber.

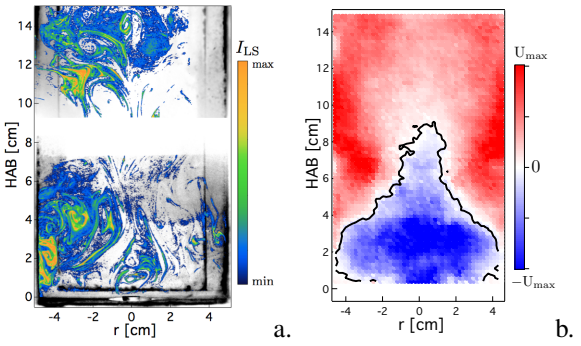

Figure 3: a) Image of light scattering intensity, indicating the instantaneous soot presence (combination of two images recorded at different instants). Parasitic background signals from light reflection on the chamber walls are not eliminated as they provide information on the chamber geometry and on the position of the bluff-body (grayscale). b) Axial velocity field derived from PIV treatment of soot light scattering fields. The black contour corresponds to null axial velocity and indicates the IRZ position.

Since soot particles are characterized by a nearly zero Stokes number, the soot pattern detected via LS contains information on the turbulent velocity field as one may reasonably assume that diffusion and thermophoresis effects are negligible. Therefore, the Particle Imaging Velocimetry (PIV) methodology is here applied to 150 pairs of soot LS fields separated by 75 μs using an adaptative PIV algorithm with a minimal interrogation areas of 32x32 pixels. The images have been obtained using a 2x400 mJ Nd:YAG laser doubled at 532 nm (10 Hz, Continuum, Powerlite SL3-PIV) and a Flow sense Eo (Dantec Dynamics) camera equipped with a 532nm filter (10nm bandwidth) to enhance the signal-to-noise ratio. The resultant axial velocity U field presented in Fig. 3b only provides qualitative information on the velocity field since, being subjected to mass and number variations, soot particles cannot be considered as "perfect" tracers. It is however possible to recognize the presence of a wide central inner recirculation zone (IRZ), identified by the black isocontour $U = 0$. Compared to a classical swirled flame, one notices the absence of outer recirculation zones close to the chamber corners. This atypical flow structure is characteristic of a toroidal swirled flame, that expands in the lateral direction and occupies a region located near the combustor bottom plane [20]. Unfortunately, this cannot be confirmed by OH* chemiluminescence since the corresponding signal is dominated by black-body radiation from the sooting flame captured by secondary rebounds of the filter [11]. However, from the OH* field obtained in the EM2Soot configuration for the richest non-sooting premixed flame, it is possible to identify a toroidal swirled flame [11], confirming results obtained for the axial velocity field and the inferred flame structure. A more precise investigation of these is however out of the scope of this work.

3.2. Time-averaged and RMS fields of f_v

The time-averaged field of soot volume fraction $\overline{f_v}$ is obtained by summing 300 images. Results are shown in Fig. 4a. As already indicated, the asymmetry of the results is due to the soot absorption of the laser sheet that enters the chamber from the left. Time-averaged results confirm that f_v is almost negligible in the middle of the chamber and takes detectable values close to the walls. The time-averaged soot volume fraction initially reaches a maximum value of 10ppb (region A for $1 <$ HAB < 5 cm), then decreases downstream at around 6ppb (region B for $5 <$ HAB < 12 cm) and finally increases again at 8ppb (region C for $12 <$ HAB < 18 cm).

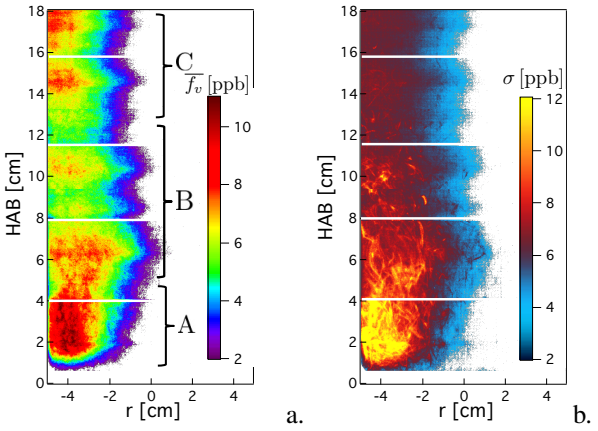

Figure 4: 2-D mapping of (a) time-averaged and (b) standard deviation of soot volume fraction from LII.

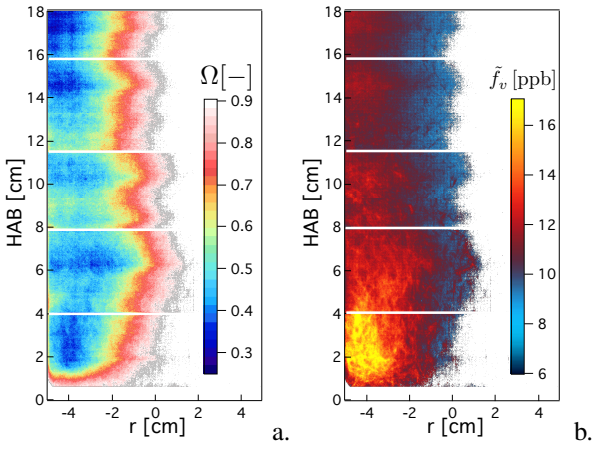

Figure 5: 2-D mapping of (a) temporal intermittency and (b) weighted time-averaged soot volume fraction field from LII.

The trend observed for $\overline{f_v}$ differs from what may be concluded from the flame luminosity image[2] in Fig. 1a. By considering the flame luminosity, one can deduce that soot is present in the whole chamber while LII measurements only detect high soot volume fraction levels along the lateral wall. However, the difference is due to the fact that the light intensity signal is integrated along the line-of-sight and cannot be compared to the planar 2-D field of f_v obtained with LII. Second, from Fig. 1a, $\overline{f_v}$ is expected to reach its maximum value near the bottom of the chamber and to rapidly decrease from that point. These conclusions are not confirmed by the LII measurements since $\overline{f_v}$ plotted in Fig. 4a features high values at HAB $\approx$ 16 cm. This definitely indicates that flame luminosity cannot be used to estimate the spatial evolution of $\overline{f_v}$ in the chamber since it is also dependent on the forth power of the temperature.
Results from the standard deviation of f_v, σ, are displayed in Fig. 4b. One finds that σ is maximum in region A and decreases in regions B and C, whereas $\overline{f_v}$ has a non monotonic behavior. This indicates a complex behavior of soot production that may be investigated by characterizing the temporal intermittency of the soot distribution.

3.3. Temporal soot intermittency and turbulence effects

Soot production in turbulent flames is known to be a highly intermittent phenomenon [6, 21, 22], which may be characterized by the intermittency index Ω [23]:

$$\Omega(x,y) = 1 - \frac{1}{N_t}\sum_{t=1}^{N_t} \mathcal{I}(x,y,t) \tag{1}$$

[2]Due to the exposure time for flame luminosity visualization (2μs), Fig. 1a contains time-averaged information.

where $\mathcal{I}(x,y,t)$ is the presence index:

$$\mathcal{I}(x,y,t) = \begin{cases} 0 & \text{if } f_v(x,y,t) < \epsilon \\ 1 & \text{if } f_v(x,y,t) \geq \epsilon \end{cases} \tag{2}$$

The 2-D intemittency index, displayed in Fig. 5, reaches its minimum in region C, indicating that soot presence is sporadic for small HAB (regions A and B), whereas soot particles are more likely to be continuously detected at higher HAB (region C). The temporal intermittency can strongly affect the interpretation of soot production trend, especially when it is based on time-averaged fields. Therefore, a weighted time-average operator $\widetilde{\cdot}$ is here introduced to take into account the intermittency of soot particles, by weighting time-averaged soot volume fraction by the presence of soot particles:

$$\widetilde{f_v}(x,y) = \frac{\sum_{t=1}^{N_t} f_v(x,y,t)\boldsymbol{I}(x,y,t)}{\sum_{t=1}^{N_t} \boldsymbol{I}(x,y,t)} \tag{3}$$

Results for the weighted time-averaged field $\widetilde{f_v}$ are shown in Fig. 5b. Compared to the $\overline{f_v}$ field, the weighted mean $\widetilde{f_v}$ is higher close to the bottom plane (region A) and slowly decreases downstream towards a nearly constant value. Evolutions with axial position of $\overline{f_v}$, Ω, $\widetilde{f_v}$ and σ variables in the near-wall region are summarized in Fig. 6. Here, each variable has been spatially averaged over a surface of 1 cm $\times$ 1 cm ($r \in [-4.9; -3.9]$ cm). The temporal and spatial evolution of soot volume fraction can be characterized by combining results from Fig. 6 with local information on the probability to detect a certain value of soot volume fraction. For this, the probability density function (PDF) of f_v for three axial positions corresponding to regions A, B and C are

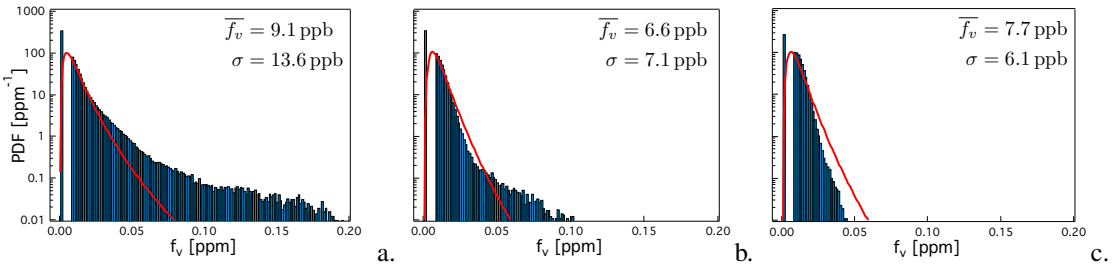

Figure 7: Evolution of the distribution of the soot volume fraction in the three zones A, B and C with the corresponding log-normal fitting curve.

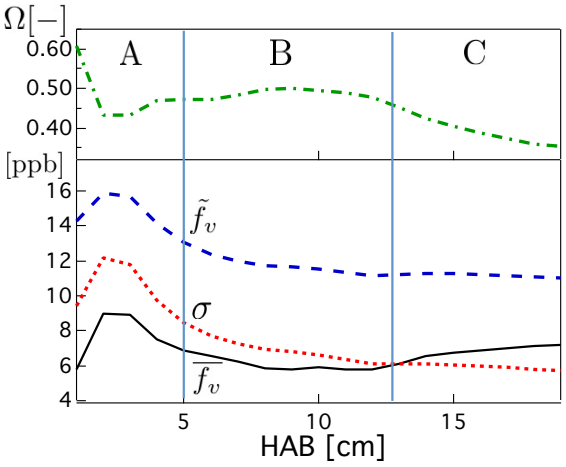

Figure 6: Axial evolution of time-averaged $\overline{f_v}$, weighted time-averaged $\tilde{f_v}$, standard deviation σ and intermittency index Ω for $r \in [-4.9; -3.9]$ cm.

shown in Fig. 7. Each histogram represents the distribution of instantaneous soot volume fraction in a square of 5×5 mm^2 centered on $r = -4.5$ cm accumulated over 300 images (HAB=3,10,17 cm). In each histogram, $\overline{f_v}$ and σ values are reported. The red line provides an estimation of the PDF for the f_v values below ϵ assuming a log-normal distribution.

Region A is characterized by a high soot temporal intermittency, indicated by the height of the first vertical bar. When soot is detected, the f_v threshold is the most probable value and, at the same time, the highest values of f_v (about 0.15 ppm) are observed in this region, leading to a maximum σ value in the center of region A (HAB= 3.5 cm). This region corresponds to the IRZ so that this behavior possibly indicates that the large eddies of the turbulent flow observed in this region in Fig. 1c induce a high variability of instantaneous f_v values. Thus, soot production can be enhanced or diminished by their actions, a feature discussed in [24, 25] for a single vortex interacting with a sooting laminar flames. Downstream, the region close to the wall for $5 <$ HAB < 12 cm (zone B) features nearly the same level of intermittency as in region A. Its most probable f_v value is close to ϵ but σ is reduced so that the final time-averaged and weighted time-averaged values are smaller than in region A. Finally, for higher HAB (region C) soot temporal intermittency is drastically reduced. Since σ is the smallest, $\overline{f_v}$ value is high again at HAB= 16 cm.

In summary, rich premixed swirled flames feature a strong relation between the spatial structure (Fig. 1c) and the temporal variability of f_v. Close to the chamber bottom corners, long ligaments of soot are wrinkled by turbulence forming large eddy soot structures with a spatial preferential concentration which temporally results in a high level of intermittency. In addition, strain rate and curvature effects induced by vortices are known to decrease or enhance soot production, respectively, increasing the variability of f_v value along a soot ligament [25]. Downstream, f_v is detectable via LII close to the wall and a quasi-homogeneous spatial distribution of soot is observed (Fig. 1c), probably due to an attenuation of the eddies strength near the wall. This results in a thinner PDF for f_v and a higher probability to detect soot as a function of time.

One may wonder whether soot oxidation plays a role in this configuration. To answer this question an attempt was made to detect OH radicals with planar laser induced fluorescence (PLIF) with a dye laser tuned to $\lambda = 282.92$ nm and detection in the band 308±5 nm (ZBPA310 Asahi bandpass filter). No signal could be detected along the height of the burner, indicating that OH volume fraction was negligible. This is in agreement with the fact that at $\phi = 2.1$ the OH concentration is expected to be quite small compared to that prevailing under stoichiometric conditions. Based on the analysis of the flame structure proposed in Section 3.1, one may consider that most of the OH concentration will be localized near the combustor bottom plane. In the absence of this radical and of oxygen (due to rich premixed con-

ditions), soot oxidation is expected to be quite limited in this configuration [11].

4. Conclusion

Soot production in turbulent flames is investigated by making use of turbulent combustion operating in the premixed mode. Experiments are carried out on a novel laboratory scale model combustor that is used to stabilize an ethylene/air rich swirling turbulent flame, established in a confined environment allowing optical access to the process. Production of soot is examined using planar laser induced incandescence (LII), providing quantitative measurements of soot volume fraction f_v along the height of the burner and planar laser light scattering (LS) by soot particles providing information on the presence and spatial geometry of soot layers. The LII reveals two important trends: soot is mainly present along the wall of the burner highlighting the role of the confinement on soot production in rich premixed flames. The evolution of the mean soot volume fraction along the height of the burner exhibits two locals maxima. The first maximum is located in the lower part of the chamber while the second is formed in the second half of the combustor at a larger distance from the injection plane. A statistical analysis of the two regions reveals that these two maximum values conceal two different trends regarding soot intermittency. Soot intermittency is highest in the lower part of the chamber and decreases along the height of the burner. A weighted mean is proposed to take into account the intermittency of soot particles leading to a rather monotonic evolution of this weighted mean along the height of the burner. Laser light scattering images combined with LII images indicate that soot particles are also present in the central region of the burner but that f_v reaches its highest values in the near wall region of the burner. The volume fraction levels in the central region are outside the dynamic range of the LII and their values are too low to be detected.

Acknowledgments

Support from G.Legros and J.Bonnety (UPMC) for the LII calibration through the MAE technique is gratefully acknowledged. This study is supported by the Air Liquide, CentraleSupelec and CNRS Chair on oxycombustion and heat transfer for energy and environment and by the OXYTEC project, grant ANR-12-CHIN-0001 of the French Agence Nationale de la Recherche.

[1] J. H. Seinfeld, Nature 391 (6670) (1998) 837–838.
[2] A. Seaton, L. Tran, R. Aitken, K. Donaldson, J. R. Soc. Interface (2009).
[3] M. Köhler, K.-P. Geigle, T. Blacha, P. Gerlinger, W. Meier, Combust. Flame 159 (8) (2012) 2620–2635.
[4] S. Y. Lee, S. R. Turns, R. J. Santoro, Combust. Flame 156 (12) (2009) 2264–2275.
[5] V. Narayanaswamy, N. Clemens, Proc. Combust. Inst. 34 (1) (2013) 1455–1463.
[6] B. Franzelli, P. Scouflaire, S. Candel, Proc. Combust. Inst. 35 (2) (2015) 1921–1929.
[7] S. Mahmoud, G. Nathan, Z. Alwahabi, Z. Sun, P. Medwell, B. Dally, Proc. Combust. Inst. 36 (1) (2017) 889 – 897.
[8] O. Park, R. A. Burns, O. R. Buxton, N. T. Clemens, Proc. Combust. Inst. 36 (1) (2017) 899 – 907.
[9] K. P. Geigle, J. Zerbs, M. Köhler, M. Stöhr, W. Meier, J. Eng. Gas Turbines Power (2011) 133 (12).
[10] K. P. Geigle, M. Köhler, W. OLoughlin, W. Meier, Proc. Combust.Inst. 35 (3) (2015) 3373–3380.
[11] M. Roussillo, P. Scouflaire, N.Darabiha, S.Candel, B. Franzelli, Proceedings of ASME Turbo Expo GT2018-76205, Lillestrom, Norway (2018).
[12] International Sooting Flame (ISF) Workshop available at http://www.adelaide.edu.au/cet/isfworkshop/.
[13] L. A. Melton, Appl. Opt. 23 (13) (1984) 2201–2208.
[14] C. Sorensen, Aerosol Sci. Technol. 35 (2) (2001) 648–687.
[15] P. Desgroux, X. Mercier, K. A. Thomson, Proc. Combust. Inst. 34 (1) (2013) 1713 – 1738.
[16] C. R. Shaddix, K. C. Smyth, Combust. Flame 107 (4) (1996) 418 – 452.
[17] G. Legros, Q. Wang, J. Bonnety, M. Kashif, C. Morin, J.-L. Consalvi, F. Liu, Combust. Flame 162 (6) (2015) 2705–2719.
[18] B. Franzelli, M. Roussillo, P. Scouflaire, J. Bonnety, R. Jalain, S. Candel, G. Legros, Proc. Combust. Inst., submitted.
[19] K. P. Geigle, R. Hadef, W. Meier, J. Eng. Gas Turbines Power (2013) 136 (2).
[20] A. Degeneve, P. Jourdaine, C. Mirat, J. Caudal, R. Vicquelin, T. Schuller, Proceedings of ASME Turbo Expo GT2018-76152, Lillestrom, Norway (2018).
[21] N. Qamar, Z. Alwahabi, Q. Chan, G. Nathan, D. Roekaerts, K. King, Combust. Flame 156 (7) (2009) 1339 – 1347.
[22] V. Narayanaswamy, N. Clemens, Proc. Combust. Inst. 34 (1) (2013) 1455 – 1463.
[23] B. F. Magnussen, Proc. Combust. Inst. 15 (1) (1975) 1415–1425.
[24] B. Cetegen, S. Basu, Combust. Flame 146 (4) (2006) 687 – 697.
[25] B. Franzelli, A. Cuoci, A. Stagni, M. Ihme, T. Faravelli, S. Candel, Proc. Combust. Inst. 36 (1) (2017) 753 – 761.